UCLA
UCLA Previously Published Works

Title

Conserved Interferon-γ Signaling Drives Clinical Response to Immune Checkpoint Blockade Therapy in Melanoma

Authors

Grasso, Catherine S
Tsoi, Jennifer
Onyshchenko, Mykola
et al.

Cancer Cell

Conserved Interferon-γ Signaling Drives Clinical Response to Immune Checkpoint Blockade Therapy in Melanoma

Graphical Abstract
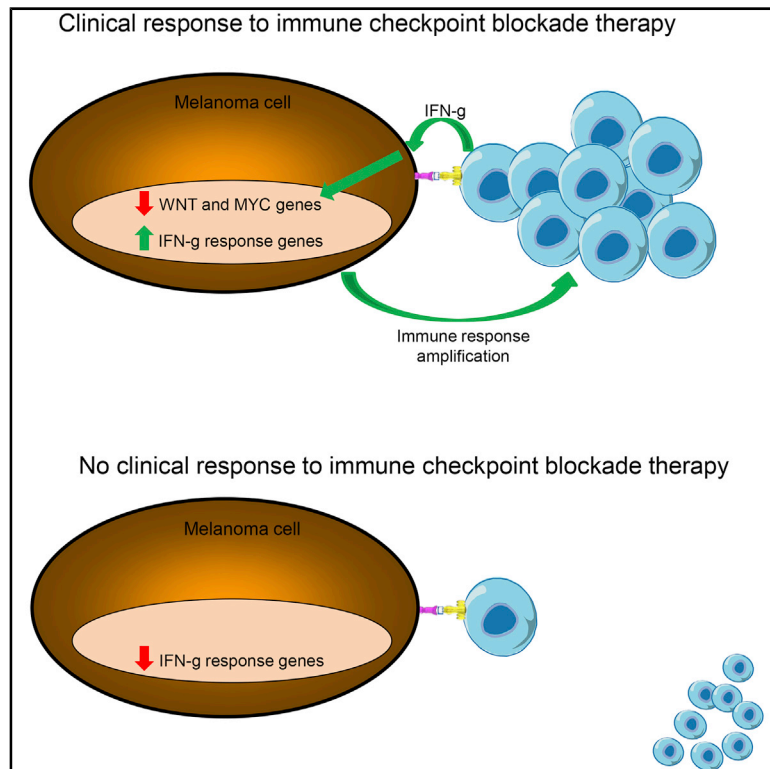
Authors

Catherine S. Grasso, Jennifer Tsoi, Mykola Onyshchenko, ..., Daniel E. Speiser, Anusha Kalbasi, Antoni Ribas

Correspondence

catherine.grasso@cshs.org (C.S.G.), aribas@mednet.ucla.edu (A.R.)

In Brief

Analyzing the transcriptome of biopsies of patients during immune checkpoint blockade therapy, Grasso et al. show that the increase of T cell infiltration and the downstream IFN-γ signaling drive clinical responses.

Highlights

- T cell-induced IFN-γ correlates the best to immune checkpoint blockade (ICB) therapy

- Immune signatures increase in on-therapy patients regardless of response to therapy

- ICB therapy decreases MYC and WNT signaling in patients with clinical response

- IFN-γ exposure of melanoma cells leads to a conserved transcriptome signature

CellPress

Article

Conserved Interferon-γ Signaling Drives Clinical Response to Immune Checkpoint Blockade Therapy in Melanoma

Catherine S. Grasso,[1,2,*] Jennifer Tsoi,[1] Mykola Onyshchenko,[1,17] Gabriel Abril-Rodriguez,[1] Petra Ross-Macdonald,[3] Megan Wind-Rotolo,[3] Ameya Champhekar,[1] Egmidio Medina,[1] Davis Y. Torrejon,[1] Daniel Sanghoon Shin,[1] Phuong Tran,[1] Yeon Joo Kim,[1] Cristina Puig-Saus,[1,5] Katie Campbell,[1] Agustin Vega-Crespo,[1] Michael Quist,[1] Christophe Martignier,[4] Jason J. Luke,[6,18] Jedd D. Wolchok,[5,7] Douglas B. Johnson,[8] Bartosz Chmielowski,[1] F. Stephen Hodi,[5,9] Shailender Bhatia,[10] William Sharfman,[11] Walter J. Urba,[12] Craig L. Slingluff, Jr.,[13] Adi Diab,[14] John B.A.G. Haanen,[15] Salvador Martin Algarra,[16] Drew M. Pardoll,[11] Valsamo Anagnostou,[11] Suzanne L. Topalian,[11] Victor E. Velculescu,[11] Daniel E. Speiser,[4] Anusha Kalbasi,[1] and Antoni Ribas[1,5,19,*]

[1]Jonsson Comprehensive Cancer Center at the University of California, Los Angeles (UCLA), Los Angeles, CA, USA
[2]Cedars-Sinai Medical Center, Los Angeles, CA, USA
[3]Translational Bioinformatics, Bristol-Myers Squibb, Hopewell, NJ, USA
[4]University of Lausanne, Lausanne, Switzerland
[5]Parker Institute for Cancer Immunotherapy, San Francisco, CA, USA
[6]University of Chicago, Chicago, IL, USA
[7]Memorial Sloan Kettering Cancer Center, New York, NY, USA
[8]Vanderbilt-Ingram Cancer Center, Nashville, TN, USA
[9]Dana Farber Cancer Institute, Boston, MA, USA
[10]University of Washington, Seattle, WA, USA
[11]Bloomberg-Kimmel Institute for Cancer Immunotherapy and Sidney Kimmel Comprehensive Cancer Center, Johns Hopkins University School of Medicine, Baltimore, MD, USA
[12]Earle A. Chiles Research Institute, Providence Cancer Institute, Portland, OR, USA
[13]University of Virginia Health System, Charlottesville, VA, USA
[14]The University of Texas MD Anderson Cancer Center, Houston, TX, USA
[15]The Netherlands Cancer Institute, Amsterdam, the Netherlands
[16]Clínica Universitaria de Navarra, Pamplona, Spain
[17]Present address: LA Biomed, Harbor-UCLA Medical Center, Torrance, CA, USA
[18]Present address: University of Pittsburgh, Pittsburgh, PA, USA
[19]Lead Contact
*Correspondence: catherine.grasso@cshs.org (C.S.G.), aribas@mednet.ucla.edu (A.R.)
https://doi.org/10.1016/j.ccell.2020.08.005

SUMMARY

We analyze the transcriptome of baseline and on-therapy tumor biopsies from 101 patients with advanced melanoma treated with nivolumab (anti-PD-1) alone or combined with ipilimumab (anti-CTLA-4). We find that T cell infiltration and interferon-γ (IFN-γ) signaling signatures correspond most highly with clinical response to therapy, with a reciprocal decrease in cell-cycle and WNT signaling pathways in responding biopsies. We model the interaction in 58 human cell lines, where IFN-γ *in vitro* exposure leads to a conserved transcriptome response unless cells have IFN-γ receptor alterations. This conserved IFN-γ transcriptome response in melanoma cells serves to amplify the antitumor immune response. Therefore, the magnitude of the antitumor T cell response and the corresponding downstream IFN-γ signaling are the main drivers of clinical response or resistance to immune checkpoint blockade therapy.

INTRODUCTION

Immune checkpoint blockade (ICB) therapy with antibodies targeting the cytotoxic T lymphocyte-associated protein 4 (CTLA-4) or the programmed cell death-1 receptor (PD-1) blocks two main negative regulators of antitumor immune responses (Curran et al., 2010; Sharma and Allison, 2015a; Wei et al., 2017) and induces durable responses in a subset of patients

with melanoma and other cancers (Ribas and Wolchok, 2018; Sharma and Allison, 2015b). Pathological studies performed in tumor biopsies from treated patients support that clinical responses induced by the use of ICB are mediated by tumor-infiltrating T cells that have been re-activated by inhibiting these immune checkpoints (Sharma et al., 2019; Tumeh et al., 2014). Transcriptomic and genomic sequencing of baseline and on-therapy biopsies from patients treated with ICB allow

for a comprehensive analysis of mechanisms underlying tumor response and resistance. As the mechanism of action is based on the interaction between immune effector cells with their cancer cell targets, these studies have to focus not only on the genetic alterations and gene expression profiles of cancer cells (Hugo et al., 2016; Liu et al., 2019; Riaz et al., 2017; Rodig et al., 2018), but they also need to analyze the composition of the immune infiltrate and its expression of immune activating gene programs (Auslander et al., 2018; Ayers et al., 2017; Cabrita et al., 2020; Chen et al., 2016; Cristescu et al., 2018; Fehrenbacher et al., 2016; Gide et al., 2019; Helmink et al., 2020; Jerby-Arnon et al., 2018; Jiang et al., 2018; Liu et al., 2019; Petitprez et al., 2020; Rodig et al., 2018; Roh et al., 2017; Sade-Feldman et al., 2018). A major focus has been on the study of biopsies from patients with advanced melanoma treated with anti-PD-1 antibodies administered alone, in sequence or in combination with anti-CTLA-4 antibodies. A study combining immunohistochemistry analyses with RNA sequencing (RNA-seq) in biopsies from patients treated sequentially with the anti-CTLA-4 antibody ipilimumab before or after the anti-PD-1 antibody nivolumab concluded that primary response to anti-CTLA-4 required high levels of major histocompatibility complex (MHC) class I expression by cancer cells at baseline, while response to anti-PD-1 was more associated with a pre-existing interferon-γ transcriptome signature (Rodig et al., 2018). Another study combining immunohistochemistry analyses with RNA-seq in tumor biopsies from patients treated with anti-PD-1 monotherapy or combined with anti-CTLA-4 confirmed the association of response to PD-1 blockade therapy with baseline evidence of activated T cells using morphological and transcriptome signatures, in particular of an effector memory T cell phenotype (Gide et al., 2019). A third study with a large cohort of baseline biopsies from patients treated with anti-PD-1 therapy, with or without prior anti-CTLA-4 therapy, revealed that response to PD-1 blockade was associated with increased MHC class I and II expression (Liu et al., 2019). In this study, whole-exome sequencing revealed occasional genetic alterations in antigen presentation machinery genes in biopsies of patients who did not respond to therapy (Liu et al., 2019).

CheckMate 038 is a prospective, multicenter, international, multi-cohort clinical trial designed to collect tumor biopsies from patients with metastatic melanoma treated with the anti-PD-1 antibody nivolumab as front-line therapy or after progressing on-therapy with the anti-CTLA-4 antibody ipilimumab, or receiving the combination of both antibodies. Biopsies of 68 patients receiving nivolumab monotherapy in part 1 of this study have been reported previously (Riaz et al., 2017). These samples were analyzed by whole-exome, transcriptome, and T cell receptor (TCR) sequencing. Data revealed increases in distinct immune cell subsets and upregulation of immune activation gene programs that was more pronounced in patients with a clinical response to therapy (Riaz et al., 2017). In this study, we provide information on the transcriptome analysis of tumor biopsies from the complete set of 101 patients treated with single-agent nivolumab or with the combination of nivolumab and ipilimumab, which is correlated with the *in vitro* analysis of how a panel of melanoma cell lines change gene expression upon exposure to interferon-γ.

RESULTS

Patient Characteristics and Response to ICB Therapy

We analyzed tumor biopsies obtained from patients treated with nivolumab or nivolumab plus ipilimumab within the CheckMate 038 study (NCT01621490), which required baseline and on-therapy biopsies from all patients. The clinical trial had several parts (Figure S1). Part 1 included two cohorts that received nivolumab monotherapy: patients whose melanomas had previously progressed on anti-CTLA-4 monotherapy, and those who were naive to prior anti-CTLA-4. In part 2, patients who were anti-CTLA-4-naïve received combination therapy with nivolumab and ipilimumab. Part 3 was also restricted to patients who were anti-CTLA-4 naïve, and randomized patients 1:2 to receive either nivolumab monotherapy or combination therapy with ipilimumab. Part 4 was similar to part 3 in being restricted to patients naive to anti-CTLA-4, but included patients with active brain metastases who received either nivolumab monotherapy or combination therapy with ipilimumab. Results of analysis of biopsies of patients from part 1 have been reported previously by Riaz et al. (2017), while analyses from parts 2–4 have not been reported previously. Biopsies were planned at baseline and during treatment (week 4 for part 1, and week 2 or 4 for parts 2–4) and were processed centrally to obtain RNA for sequencing analyses.

Among the 170 patients enrolled in the clinical trial (Figure 1A), 106 patients received nivolumab alone and 62 received nivolumab and ipilimumab combined therapy. RNA was isolated from 101 baseline and 99 on-therapy biopsies (Figure 1A). Several biopsies were not included in this analysis for different reasons, including specimens not meeting quality standards, patients who received a treatment that was not assigned, not having adequate tumor response assessment, and a diagnosis of primary choroidal melanoma (eight patients) due to the distinct biology of this uncommon melanoma subtype (Figure 1A). At the end, there were 84 baseline and 85 on-therapy biopsies (68 of which were paired), that contributed to transcriptome analyses for RNA-seq (Figure 1A). Table 1 shows the clinical characteristics of the analysis cohort, including 101 total patients: median age was 56 years (range 22–89 years). The majority (71%) of patients had cutaneous melanoma, with 11% mucosal and 4% acral melanoma. The majority of patients had stage IV disease (93%), and the adverse prognosis factor of increased lactate dehydrogenase was present in 28% of patients.

CheckMate 038 was not designed to assess comparisons between study groups as these were mostly non-randomized cohorts (Figure S1). Therefore, the account of tumor responses and time-to-event outcomes is descriptive and used for the interpretation of the tumor biopsy analyses. Overall, there were more patients with an objective response (complete response or partial response [CRPR]) in the group receiving the combination of nivolumab and ipilimumab than among patients treated with nivolumab monotherapy, whether or not naive to anti-CTLA-4 therapy (Figure 1B). Analyses of overall survival (OS) and progression-free survival (PFS) suggested that survival outcomes were similar among patients receiving nivolumab monotherapy, whether or not they had received prior anti-CTLA-4; OS and PFS among patients receiving combination nivolumab plus ipilimumab therapy appeared to exceed nivolumab monotherapy
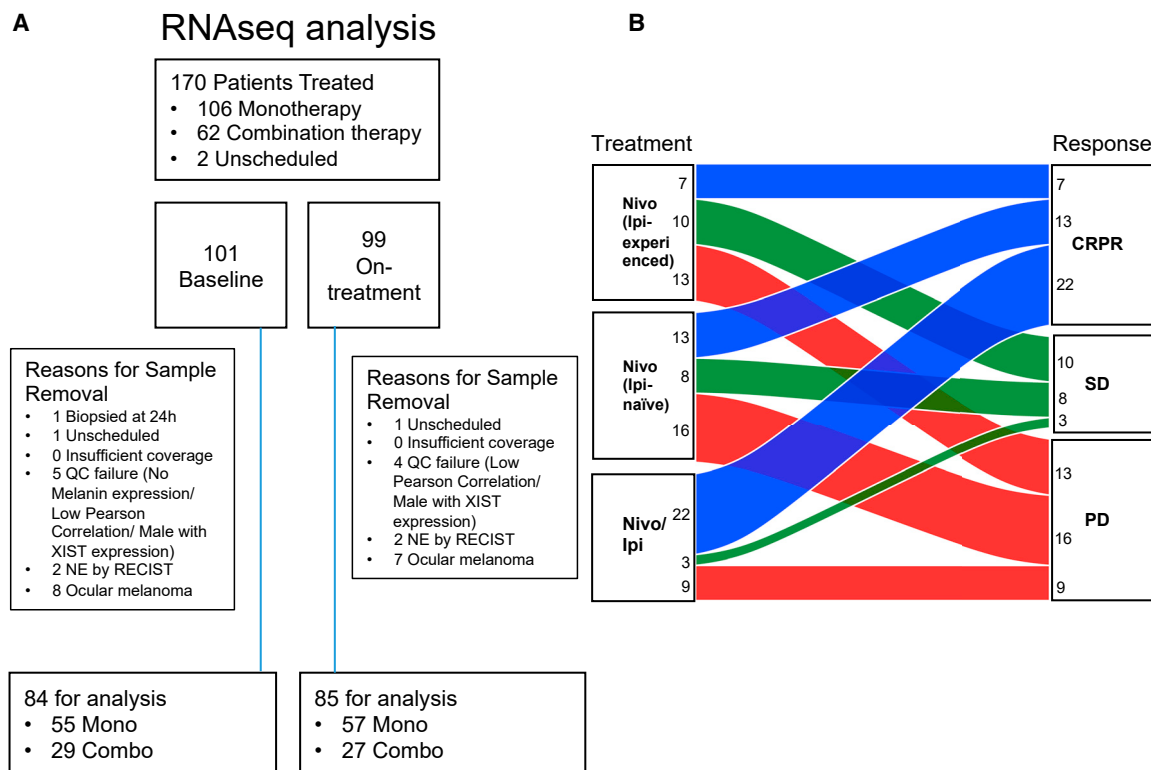
Figure 1. Outline of Sample Collection, Patient Treatments, and Response to Therapy
(A) Consort diagram describing data generation and selection of final transcriptome cohort.
(B) Alluvial plot showing the number of patients of each treatment subtype that resulted in each response. The numbers in the treatment subtype box represent the number of patients of that treatment type who had that response (red, PD; green, SD; blue, CRPR).
See also Figures S1 and S2.

outcomes (Figure S2A). When analyzing OS and PFS according to tumor response assessment, patients with CRPR unsurprisingly had prolonged survival compared with those with stable disease (SD) or progressive disease (PD) (Figure S2B). Based on these observations, for the RNA-seq analyses we compared patients receiving combination therapy to those receiving nivolumab monotherapy (merging the groups that had or had not previously received ipilimumab), and clinical response was defined as CRPR compared with SD or PD.

The Dominant Signal Associated with Response or Resistance to ICB Therapy in Patient Biopsies Is Mediated by T Cells
Consistently, it has been shown that high levels of CD8 T cell infiltration of tumors at baseline and on-treatment are predictive of clinical response to ICB in patients with advanced melanoma (Chen et al., 2016; Gide et al., 2019; Tumeh et al., 2014). We used the method denominated microenvironment cell populations-counter (MCP-counter) (Becht et al., 2016) for RNA-seq data deconvolution to define immune cell types. We applied an optimal pooled t test, since only a subset of the samples were paired. Using these approaches, we documented that biopsies of patients with a response to therapy had higher baseline levels of T cells than those with PD (Figure 2A). They also had significantly higher baseline levels of B lineage cells, myeloid dendritic cells, and natural killer cells (Figure 2A). The

change from baseline to on-therapy was greater in biopsies of patients with a response to therapy, and there were increases in T cell infiltrates in biopsies of patients whether or not they had an objective clinical response to therapy, and regardless of receiving combination therapy or nivolumab alone (Figures 2A and 2B).

With the goal to define the main drivers explaining the overall biopsy data, we then analyzed the whole-transcriptome RNA-seq dataset using principal-component analysis. Analysis of the first two principal components showed that the signature for T cell score derived from MCP-counter RNA-seq data deconvolution was the main factor organizing the data, and it segregated with response to therapy (with the exception of 19 outlier samples, 12 of which were matched from the same patients with baseline and on-therapy biopsies, Figure 2C). Of note, in previous work we had validated the MCP-counter T cell score with pathological analysis of immune infiltrates in corresponding patient biopsies (Grasso et al., 2018). In the CheckMate 038 biopsy dataset, the best organization of the samples was according to the degree of T cell infiltration regardless of whether this was observed in baseline or on-therapy biopsies, with or without prior treatment with ipilimumab, single or combination ICB therapy, as well as clinical response or no response to therapy, with the paired CRPR samples showing the most consistent alignment along the T cell score vector (Figures 2C and 2D). Figure S3 shows the degree to which the T cell score dominates the

Table 1. Baseline Patient Characteristics

	n (%) N = 101
Age (years)	
Median	56
Range	22–89
Sex, n (%)	
Male	58 (57.4)
Female	43 (42.6)
ECOG performance status, n (%)	
0	70 (69.3)
1	29 (28.7)
Not reported	2 (2.0)
Stage at study entry, n (%)	
III	8 (7.9)
IV	93 (92.1)
Prior anti-CTLA-4 therapy, n (%)	
Yes	30 (29.7)
No	71 (70.3)
***BRAF* mutation status, n (%)**	
Positive	33 (32.7)
Negative	61 (60.4)
Not reported	7 (6.9)
PD-L1 status at baseline, n (%)	
PD-L1 negative (TPS baseline = 0)	30 (29.7)
PD-L1 positive (TPS baseline >0)	48 (47.5)
NA (TPS baseline = NA)	23 (22.8)
Metastatic staging, n (%)	
M0	2 (2.0)
M1A	17 (16.8)
M1B	15 (14.9)
M1C	53 (52.5)
Not reported (stage III)/unknown	14 (13.9)
Brain metastases, n (%)	
Yes (*)	13 (12.9)
No	80 (79.2)
Not reported (stage III)	8 (7.9)
Lactate dehydrogenase, n (%)	
Normal ($\leq$ULN)	72 (71.3)
Elevated (>ULN, $\leq$2*ULN)	24 (23.8)
Highly elevated (>2*ULN)	4 (4.0)
Not reported	1 (1.0)
Melanoma primary site, n (%)	
Acral	4 (4.0)
Cutaneous	71 (70.3)
Mucosal	11 (10.9)
Other	15 (14.9)

ECOG, Eastern Cooperative Oncology Group; M1a, metastases to skin, subcutaneous tissues, or distant lymph nodes; M1b, metastases to lung; M1c, metastases to all other visceral sites or distant metastases at any site combined with an increased serum concentration of lactate dehydrogenase; PD-L1, programmed death ligand 1.

*In addition to all patients enrolled in part 4, a number of patients in parts 1–3 also had reported brain metastases.

data, with the large number of genes correlated (n = 2,047) and anti-correlated (n = 1,087) with this score based on a Pearson correlation cutoff of ±0.3. This supplemental figure also includes information about the effect of the melanoma subtype (cutaneous, mucosal, or acral) on the tumor transcriptome. The coordinated alignment of the correlated and anti-correlated genes on-treatment is reflected in the significant upregulation of the correlated genes and the significant downregulation from baseline to on-treatment in CRPR biopsies (optimal pooled t test p < 1×10^{-4} and p < 1×10^{-4}, respectively, Figure 2C). The correlated genes accounted not only for systematic changes in the tumor cell gene expression, but also in the tumor microenvironment. Except for neutrophils, the MCP-counter immune cell signatures were highly correlated with the T cell signature (R^2 $\geq$ 0.6, Figures S4A and S4B). Use of t-SNE embedding to cluster genes with their closest MCP-counter immune cell signature resulted in only two main clusters: genes that correlated with the T cell score and genes that were anti-correlated (Figure S4C). These data indicate a truly coordinated immune response, including large numbers of genes, which was dominated by changes in T cells. We acknowledge that this conclusion is limited by being derived from bulk RNA-seq analyses as opposed to single-cell RNA-seq. Based on these analyses, we conclude that ICB therapy has the potential to increase T cell infiltrates regardless of whether there are clinical responses to therapy, and that a greater degree of T cell infiltrate increases from baseline to on-therapy biopsies is associated with improved response to therapy.

Interferon-γ Response Genes Play an Integral Role in Response and Resistance to Therapy as Mediators of the T Cell Program

We examined the expression of effector cytokines and toxic granules induced by TCR engagement with cognate antigen, including the cytotoxic molecules perforin and granzyme B, tumor necrosis factor alpha (TNF-α) family members FAS, TRAIL (TNFSF10), and TNF-α, and interferon-γ, applying an optimal pooled t test. The expression of perforin, granzyme B, TRAIL, and TNF-α followed the pattern of expression of interferon-γ, and was higher in biopsies of patients with a clinical response to therapy (Figure S5). As exposure to most of these molecules results in cytotoxic death of cancer cells, we reasoned that the cancer cell expression of interferon response genes may be relevant to attracting other immune cells into the tumor microenvironment and amplifying the antitumor immune response once it is initiated.

Melanoma Cells Have a Uniform Gene Set Response to Interferon-γ Provided That They Can Signal through the Interferon-γ Receptor

With the goal of addressing the question if differential responses to ICB may be due to a different inherent ability of melanoma cells from different patients to respond to interferon-γ, we set
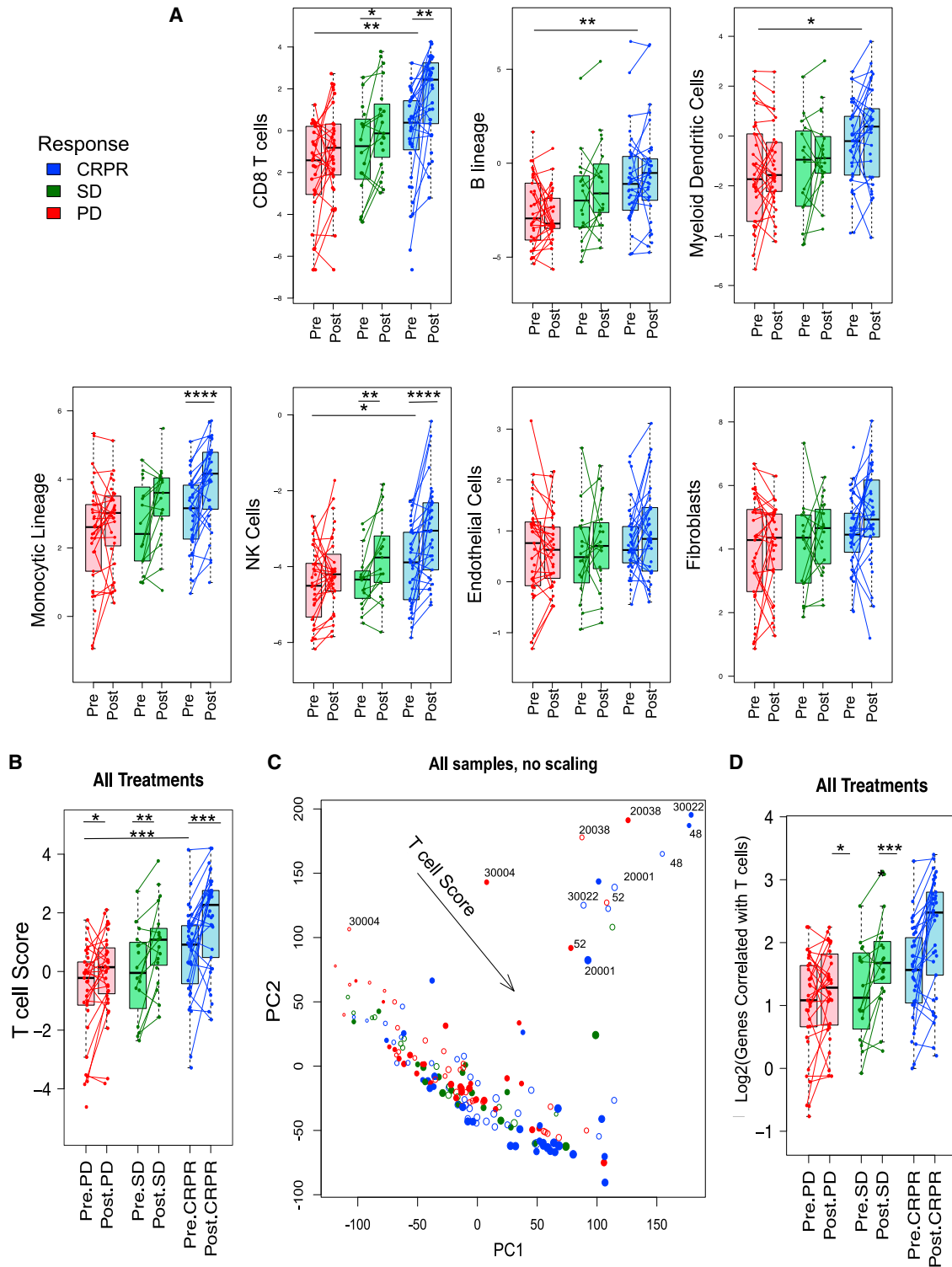
Figure 2. Immune Cell Infiltration in Patient Samples from Clinical Study CheckMate 038

(A) Boxplot the MCP-counter T cell score according to response to therapy combining all treatment groups using an optimal pooled t test since data are paired and unpaired.

(B) Boxplots showing the average expression of the genes correlated with the T cells broken down by response and pre- and on-treatment using an optimal pooled t test since data are paired and unpaired.

out to examine the transcriptome changes in a panel of *ex-vivo*-cultured melanoma cells exposed to interferon-γ. For this study, we used 57 previously established and described cell lines from cultures of human melanoma biopsies or surgical resections (Atefi et al., 2014; Neubert et al., 2017; Shin et al., 2017; Tsoi et al., 2018) and the primary melanocyte line, HeMa, as a non-malignant pigmented cell control. This cell line panel included three variants of corresponding parental melanoma cell lines that had been rendered resistant to BRAF inhibitors by continuous *in vitro* drug exposure, denoted as AR for acquired resistance (Atefi et al., 2014; Nazarian et al., 2010; Tsoi et al., 2018); three cell lines that had developed Janus kinase 1 (*JAK1*) or *JAK2* loss-of-function mutations in patients; as well as variants of parental cell lines that had *JAK1* (N = 5), *JAK2* (N = 5), or beta-2 microglobulin (*B2M*) (N = 2) loss of function generated *in vitro* through CRISPR-Cas9 gene editing, as these are genetic events known to be associated with resistance to anti-PD-1 therapy (Garcia-Diaz et al., 2017; Gettinger et al., 2017; Sade-Feldman et al., 2017; Shin et al., 2017; Sucker et al., 2017; Torrejon et al., 2020; Zaretsky et al., 2016). These cell lines were exposed to 5 ng/mL of interferon-γ for 6 h to assess immediate whole-transcriptome changes by RNA-seq analysis.

We found that a cell line's gene expression profile was most correlated with itself at baseline and upon exposure to interferon-γ, indicating that cell line identity is a major contributor to gene expression (Figure S6). In addition, we observed that the baseline samples were not correlated with each other, nor were the interferon-γ-exposed samples correlated with each other (Figure S6). However, for the 46 cell lines that responded to interferon-γ, the changes between on-treatment and baseline for interferon-γ were highly correlated as a result of consistent large changes in interferon-γ response genes (Figure S7). Figure S8A shows the high level of concordance among expression changes of known interferon-γ response genes, making it possible to identify outlier gene expression changes, such as the two samples whose *JAK2* expression decreased significantly compared with the rest of the samples. Analysis of all increased and decreased gene expression showed that there were two broad groups of cell lines: the great majority (n = 46) that could signal through the interferon-γ receptor and had large changes in the expression of the same set of interferon-γ response genes; and a distinct set of 12 cell lines that had *JAK1* or *JAK2* natural or induced loss-of-function mutations and were largely unable to signal through the interferon-γ receptor (Figures 3 and S8B). Of note, there were no major differences in gene expression profiles induced by interferon-γ exposure in cell lines with acquired resistance to BRAF inhibitors or in *B2M* knockout cell lines. Therefore, this large panel of melanoma cell lines, each of which had a unique gene expression signature, responded consistently to interferon-γ exposure.

To identify a set of genes up- and downregulated in response to interferon-γ in typical melanoma cell lines, we used all the samples that were not experimentally modified (excluding cases with *JAK1*, *JAK2*, and *B2M* loss generated by CRISPR-Cas9, as well as the *AR* samples but including naturally occurring *JAK* and *B2M* loss cases). We performed a paired t test between cell lines before and after treatment with interferon-γ and observed a significant decrease in the expression of 1,176 genes and increase in the expression of 549 genes after applying a false discovery rate (FDR) cutoff of 0.01. These changes clustered with the changes in the primary melanocyte line HeMa, included as a normal control, indicating that normal interferon-γ signaling was intact in all of these cases (Figure S8B). This transcriptome signature includes previously reported interferon-γ response genes, melanoma-specific responses, as well as a deeper look into the genes whose expression decreases in response to interferon-γ (Figure S9).

Interferon-γ Triggers Melanoma Cells to Increase Expression of Interferon Pathway Genes, Antigen Presenting Machinery, and T Cell-Attracting Chemokines

We next focused the analysis on changes in known genes that are related to interferon-γ exposure, including interference with cell proliferation (the first functional effect that led to the description of interferons), upregulation of antigen presentation machinery, enhancement of immune cell-attracting chemokines, as well as genes involved in positive and negative downstream interferon signaling pathways (Bach et al., 1997). Figure 3A shows the response as fold changes, while Figure S10 shows it in terms of baseline and on-treatment gene expression. The overall change in transcripts involved in cell proliferation was low after 6 h of *in vitro* interferon-γ exposure (Figure 3A). There was evidence of increased expression of multiple *HLA* class I and II genes, with the most consistent increase being in *HLA-E*. The two major clusters in the data were defined by whether or not *HLA* class II genes are expressed at baseline. There was a very strong and consistent increase in the expression of additional genes in the antigen presentation pathway, in particular *NLRC5* (also known as HLA class I transactivator) and *CIITA* (HLA class II transactivator), *TAP* transporters and proteasome subunits. Another set of genes with large increases were those involved in the interferon signaling pathway itself, representing an amplification of the interferon-γ signal, including *JAK2* (but not *JAK1*), several signal transductors and activators of transcription and interferon response factors (*IRFs*), in particular the transcription factor *IRF1*, which serves as a well-defined positive control gene of interferon-γ response (Garcia-Diaz et al., 2017), going up in all the samples with *JAKs* intact (Figure 3B). With this gene group, there was also an increase in negative

(C) Principal-component analysis showing all RNA-seq samples, paired and unpaired, plotted on the first two components. The size of the data point is proportional to the T cell score. Open circles correspond to pre-treatment samples, while closed circles correspond to on-treatment samples. The data points are colored by response (red, PD; green, SD; blue, CRPR). The vector for the T cell score is plotted as well. Outlier samples are labeled by case. The 12 paired outlier samples were either due to quality control issues that had not been detected, or may be due to an actual different biology. For example, cases 48, 20038, and 30022 all had interferon-γ signaling either going down or not changing on-treatment, while cases 30004 and 20001 have G2M cell-cycle genes that either increase or did not respond.

(D) Boxplots of MCP-counter immune cell deconvolution types according to response to therapy.

Mixed t test for paired and unpaired samples using an optimal pooled t test since data are paired and unpaired (*p < 0.05, **p < 0.01, ***p < 0.001, ****p < 0.0001). See also Figures S3–S5.
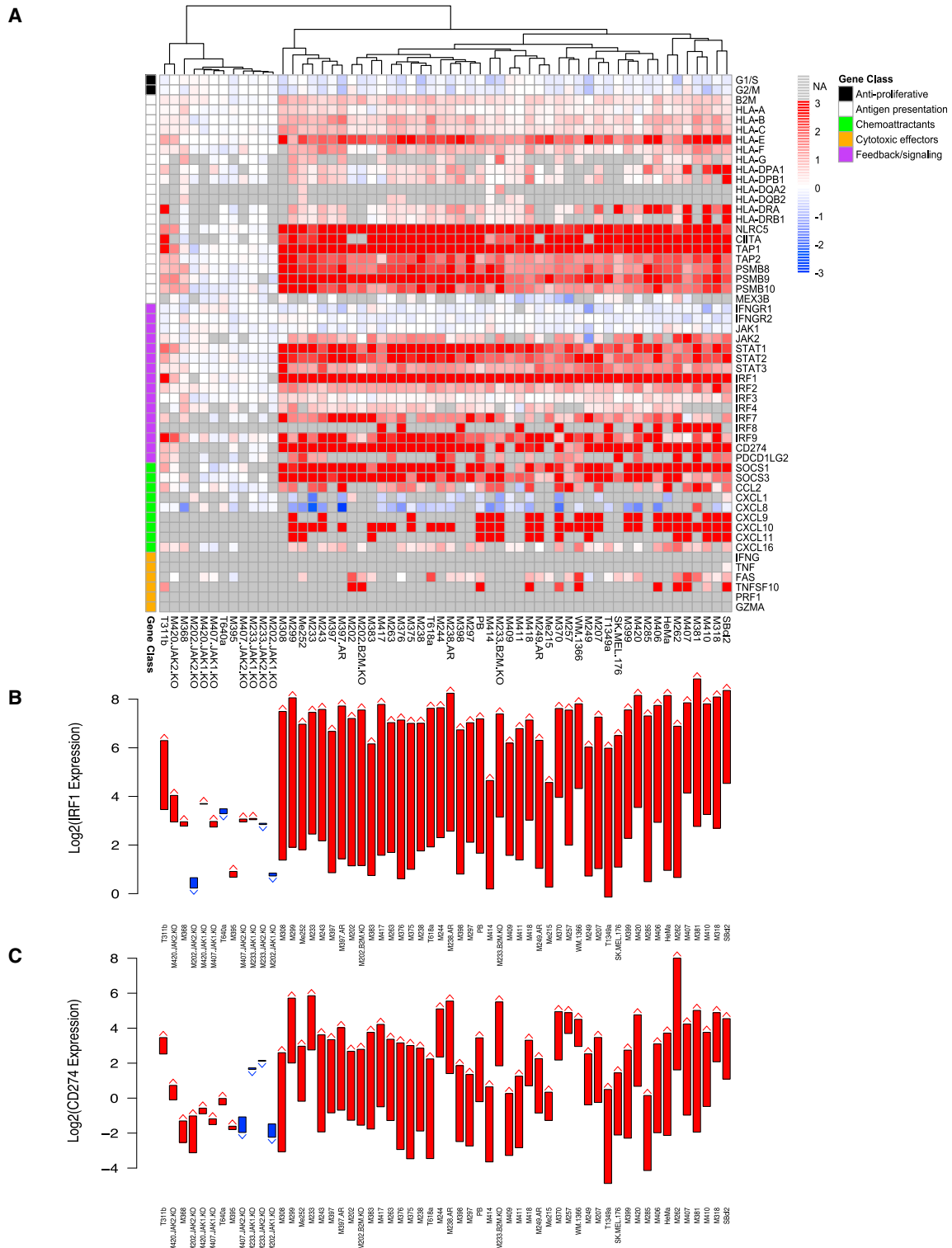
Figure 3. Interferon-γ-Induced Changes in Gene Expression in 58 Human Cell Lines

(A) Heatmap of changes in key interferon-γ response genes after 6 h of treatment at 5 ng/mL expressed as fold changes pre-treatment to post-treatment. Genes are organized by class: anti-proliferative (black), antigen presentation (white), chemoattractants (cyan), cytotoxic effectors (orange), feedback/signaling (purple).

(B) The pre- and post-treatment gene expression levels of *IRF1*, the transcription factor executing the downstream interferon-γ program, shown as arrows (red, up; blue, down).

(C) The pre- and post-treatment gene expression levels of *CD274*, the gene that codes for PD-L1, shown as arrows (red, up; blue, down).

See also Figures S6–S10.

regulators of the pathway including *SOCS* genes, as well as *PD-L1* (*CD274*), which are also well characterized interferon-γ immediate response genes (Garcia-Diaz et al., 2017; Shin et al., 2017) (Figure 3C). Chemokines, in particular *CXCL9*, *CXCL10*, and *CXCL11*, were increased more consistently than immune effector molecules and physiologically serve to attract more T cells in response to interferon-γ exposure. These increases in gene expression were very inconsistent or non-existent in the 12 cell lines that had *JAK1* or *JAK2* natural or induced loss-of-function mutations. Overall, melanoma cell lines have a near uniform transcriptome response to interferon-γ exposure, with increases in transcripts for antigen presentation, interferon pathway, and chemokine genes, that is lost if there are loss-of-function mutations in interferon-γ receptor pathway signaling at the level of *JAK1* or *JAK2*.

Analysis of Interferon-γ Response Genes in Patient Biopsies Reveals Increased *HLA* Expression as the Major Difference between Response and Lack of Response to ICB Therapy

We analyzed the CheckMate 038 patient biopsies for interferon-γ response genes before and during ICB therapy. For this analysis, we acknowledge that cells other than melanoma cells may be responsible for the expression of interferon-γ response genes when analyzing bulk RNA-seq from biopsies as opposed to the experiment using human cell lines or single-cell RNA-seq from fresh tumor biopsies. Biopsies of patients with PD and SD included samples with and without expression of interferon response genes at baseline (Figure 4). There was evidence of an increase in the frequency and intensity of gene expression in on-therapy biopsies, in particular for chemokines and immune effector molecules (Figure 4). Biopsies of patients with CRPR had higher baseline expression of interferon response genes, which increased substantially in the on-therapy biopsies (Figure 4). The largest difference between the PD and SD groups compared with the CRPR group was in the marked increase in antigen presentation pathway genes, in particular in *HLA* class I and class II genes, *B2M*, *TAP1*, *TAP2*, *NLRC5*, and *CIITA*. After normalizing the data by leukocyte common antigen ([LCA], CD45 gene) expression to account for changes in immune cell infiltrates, the HLA class I gene expression did not increase. This does not mean that it did not increase in the tumor, but rather that the predicted increase in HLA class I expression due to interferon-γ signaling was not large enough to be detected against the background of other changes in the tumor microenvironment (Figures S11 and S12). Therefore, the main difference between interferon-γ genes in biopsies of patients with response and resistance to ICB was an increase in antigen presentation genes in biopsies obtained during therapy, a conclusion that can be confounded by being derived from bulk RNA-seq analyses.

CRPR Cases Were Associated with Consistent Changes in Hallmark Pathways, While PD Cases Involve Different Pathways for Each Sample

We found a large set of genes that were significantly different between on-treatment CRPR and on-treatment PD, likely driven in part by the large number of consistent changes in the on-treatment CRPR relative to the pre-treatment CRPR (1,935 up and 3,503 down after applying an optimal pooled t test with an FDR cutoff of 0.05, Figure S13). The SD and PD samples did not change consistently from pre-treatment to on-treatment, except for four genes, *ADI1*, *ARHGEF9*, *POU6F2*, and *RGPD4*, which were significantly different on-treatment relative to pre-treatment SD cases (after applying an optimal pooled t test with an FDR cutoff of 0.05). Only one gene in baseline samples was associated with response, as expression of *GPR31* was significantly different between biopsies of patients with CRPR or PD (p = 8.4 × 10^{-7}, after applying an optimal pooled t test with an FDR cutoff of 0.05).

To understand the major pathways driving response or lack of response, we applied gene set enrichment analysis (GSEA) using the hallmark gene signatures to identify enrichment of gene sets changing on-treatment in CRPR (Figure 5A). We identified a set of gene signatures that were also present when we applied GSEA to genes significantly altered in cell lines after interferon-γ treatment (Figure 5B). When analyzed individually for the two top-scoring pathways according to response to therapy, most biopsies with CRPR had increases in interferon-γ genes and decreases in G2M checkpoint genes, while biopsies from patients with PD had increases or decreases of these gene sets with no apparent directionality (Figure S14). This implies that interferon-γ response, presumably resulting from higher tumor antigen-specific T cell infiltration, is the major driver of clinical response in the CRPR samples. Despite the caveat of the mixed cell content of the tumor microenvironment contributing to the bulk RNA-seq transcriptome analysis, the CRPR and SD cases had high increases in interferon-γ response gene sets that were consistent with the interferon-γ 6 h *in vitro* human cell line data, while there were PD cases for which all the interferon-γ genes were downregulated (Figures S14 and S15). Similarly, for the HALLMARK_G2M_CHECKPOINT gene set, most of the CRPR and SD cases were decreased, consistent with the interferon-γ 6-h *in vitro* exposure data (Figures S14 and S15). However, there were biopsies from multiple patients with PD and one with SD for which all the cell-cycle genes increased. Other individual Hallmark gene sets similarly revealed fold changes consistent with interferon-γ treatment for CRPR cases, while changes for the PD cases were the opposite of what would be expected based on interferon-γ biology. This is true both for additional immune gene sets (Figures S16 and S17) and for additional cell-cycle gene sets for E2F targets and mitotic spindle (Figure S18). The main observation was that the gene expression profile of biopsies from patients with clinical response is well defined and consistent with exposure to interferon-γ, while there was a large diversity of gene expression changes in SD and PD cases.

Changes in WNT, MYC, and T Cell Exclusion Programs as Tumor-Intrinsic Responses to Interferon-γ

Several publications have recently shown that high WNT signaling contributes to immune exclusion (Grasso et al., 2018; Luke et al., 2019; Nsengimana et al., 2018; Spranger et al., 2015; Spranger and Gajewski, 2018). We used a nine-gene RNA-seq-based WNT score to assess the level of WNT signaling in each biopsy (Nsengimana et al., 2018). The WNT score is the geometric average of *APC*, *APC2*, *CTNNB1*, *MYC*, *SOX11*, *SOX2*, *TCF12*, *TCF7*, and *VEGFA*. Analysis of WNT gene score revealed that biopsies of patients with CRPR exhibited a
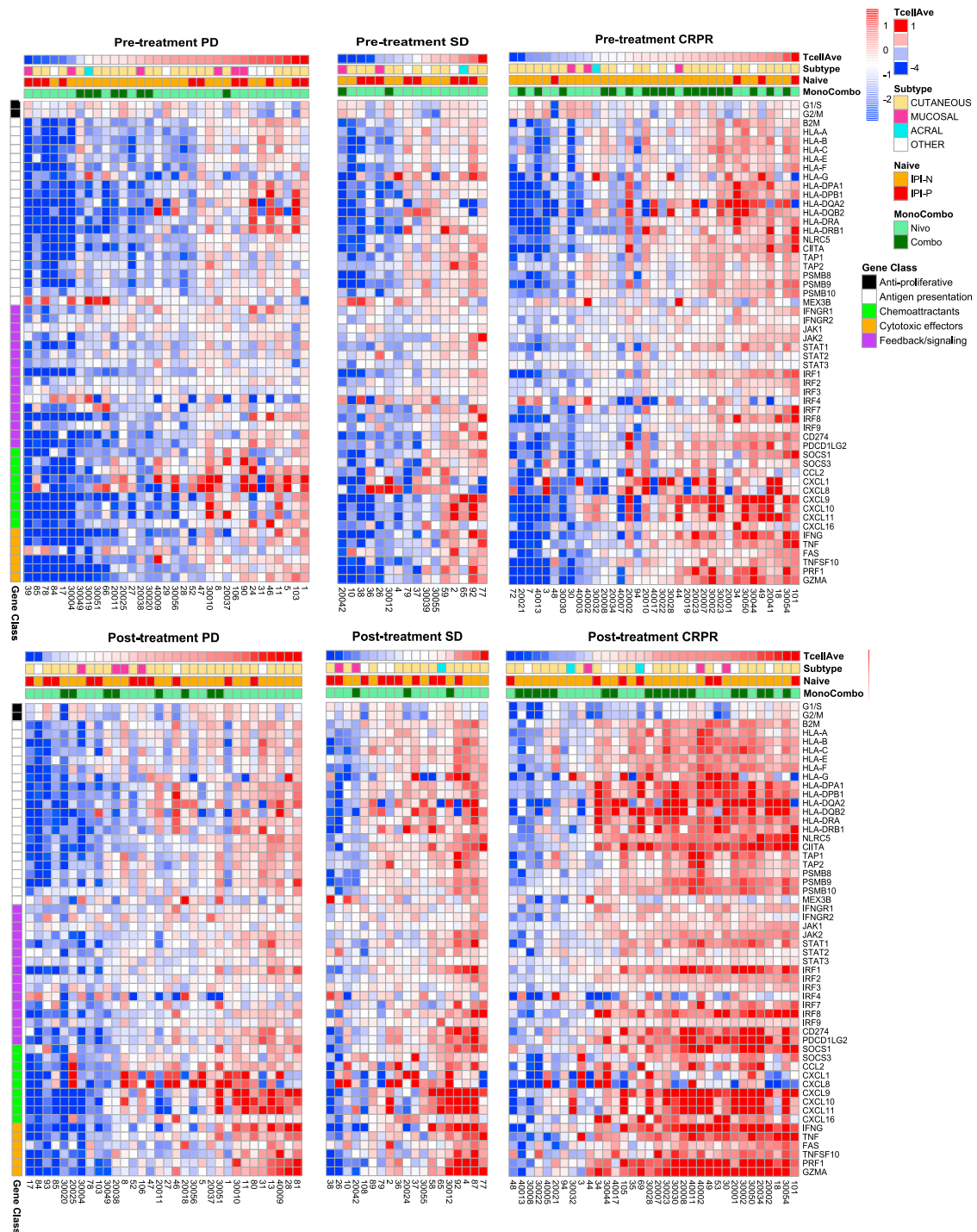
Figure 4. Interferon-γ-Induced Changes in Gene Expression in Specimens in Clinical Study CheckMate 038
Heatmap of key interferon-γ response genes in biopsies obtained at baseline and on-treatment with immune blockade therapy, separated by response to therapy. Samples are ordered by T cell score and annotated by ipilimumab naive status, monotherapy versus combination therapy and melanoma subtype. Genes are organized by class: anti-proliferative (black), antigen presentation (white), chemoattractants (cyan), cytotoxic effectors (orange), feedback/signaling (purple).
See also Figures S11 and S12.

A

Significantly Up and Down Genes in T-test for CRPR Pre to Post

HALLMARK_INTERFERON_GAMMA_RESPONSE
HALLMARK_ALLOGRAFT_REJECTION
HALLMARK_INFLAMMATORY_RESPONSE
HALLMARK_INTERFERON_ALPHA_RESPONSE
HALLMARK_COMPLEMENT
HALLMARK_TNFA_SIGNALING_VIA_NFKB
HALLMARK_IL2_STAT5_SIGNALING
HALLMARK_IL6_JAK_STAT3_SIGNALING
HALLMARK_MYC_TARGETS_V1
HALLMARK_E2F_TARGETS
HALLMARK_G2M_CHECKPOINT
HALLMARK_MYC_TARGETS_V2
HALLMARK_MTORC1_SIGNALING
HALLMARK_OXIDATIVE_PHOSPHORYLATION
HALLMARK_DNA_REPAIR

0 20 40 60 80 100 120 140 160 180 200

■ # Genes in Overlap   ■ # Remaining Genes in Gene Set

B

Significantly Up and Down Genes in T-test for IFNG 6h Treatment

HALLMARK_INTERFERON_GAMMA_RESPONSE
HALLMARK_INTERFERON_ALPHA_RESPONSE
HALLMARK_TNFA_SIGNALING_VIA_NFKB
HALLMARK_ALLOGRAFT_REJECTION
HALLMARK_COMPLEMENT
HALLMARK_INFLAMMATORY_RESPONSE
HALLMARK_IL6_JAK_STAT3_SIGNALING
HALLMARK_IL2_STAT5_SIGNALING
HALLMARK_G2M_CHECKPOINT
HALLMARK_MYC_TARGETS_V1
HALLMARK_E2F_TARGETS
HALLMARK_MITOTIC_SPINDLE
HALLMARK_UV_RESPONSE_DN
HALLMARK_ESTROGEN_RESPONSE_EARLY
HALLMARK_MTORC1_SIGNALING

0 20 40 60 80 100 120 140 160 180 200

■ # Genes in Overlap   ■ # Remaining Genes in Gene Set

Figure 5. Global Changes in Gene Expression in Clinical Study CheckMate 038 Consistent with Interferon-γ-Induced Changes in Biopsies from Patients with Response but Not without Response to Therapy

Gene set enrichment analysis (GSEA) using hallmark gene sets for significantly up- or downregulated genes for CRPR post-treatment relative to pre-treatment for clinical dataset CheckMate 038 (A) and significantly up- or downregulated genes for interferon-γ 6-h treatment for the unmodified human cell lines (B). At most 2,000 of most significant genes by q value submitted to GSEA for each class (maximum set by GSEA).

See also Figures S13–S18.

consistent significant decrease in WNT score in the on-therapy biopsies, while there was no change in the score in biopsies of patients with SD or PD (after applying an optimal pooled t test) (Figure 6A). To explore if this effect was correlated with the degree of change in T cell infiltration, we plotted the WNT score with T cell infiltration by RNA-seq deconvolution with baseline and on-therapy biopsies tracked with arrows. Again, we acknowledge that this analysis is limited by the bulk RNA-seq that includes cellular changes in the tumor microenvironment in responding biopsies, which may make it harder to interpret the results. Despite this caveat, we noted that biopsies of patients with PD or SD had a rather random distribution in this WNT/T cell space, while the majority of biopsies from patients with CRPR had a trend of going from a high WNT/low T cell to a low WNT/high T cell when comparing the baseline and on-therapy biopsies (Figure 6B). A key advantage of the data derived from the cell lines before and after exposure to interferon-γ *in vitro* was that the results were not confounded by tumor purity. We observed the same significant downward trend in the WNT gene score (p < 7.8 × 10^{-6} after applying a paired t test) in the interferon-γ responsive melanoma cell lines (Figure 6C), as six of the genes comprising the nine gene WNT score were significantly decreased in response to interferon-γ exposure. *MYC*, a WNT target gene used to monitor changes in *WNT* signaling, was similarly downregulated in response to interferon-γ exposure across most samples (Figures 6D and S19). Upstream WNT signaling genes also changed consistently in response to interferon-γ exposure, including *DKK1* and the *frizzled* gene family (Figure S20A). In fact, upregulation of *FZD5* was one of the highest increases across all samples (Figure S20B).

Expression of Genes that Drive Immune Exclusion Are Selectively Decreased in Biopsies during Response to Therapy

Recently, Jerby-Arnon et al. (2018) developed an immune exclusion signature by single-cell RNA-seq of melanoma cells from biopsies with low levels of immune infiltration. This work identified a set of transcripts originating from tumor cells that were positively or negatively associated with immune exclusion by that tu-

mor. Figure S21 shows a heatmap of these two sets of genes for the CheckMate 038 dataset. CRPR cases showed a significant decrease in the immune excluded-high genes (p < 1.4 × 10^{-4}, after applying an optimal pooled t test, Figures 6F and 6G). These genes did not change significantly in response to interferon-γ in our *in vitro* testing in melanoma cell lines (the immune excluded-down genes do go up significantly, p < 0.006, after applying a paired t test). We similarly observed significant downregulation in *CDK4* restricted to CRPR cases (after applying an optimal pooled t test, Figure 6H), which was reported as the driver of the immune exclusion signature (Jerby-Arnon et al., 2018). Based on our melanoma cell line cohort, interferon-γ does not appear to significantly alter *CDK4* expression. On the other hand, *MYC* genes followed the same pattern (after applying an optimal pooled t test, Figure 6I), consistent with the *WNT* gene score (Figure 6A), while also going down significantly in response to interferon-γ. We previously reported, using a separate set of biopsies, that *PAK4* was overexpressed in biopsies of patients with low T cell infiltration and lack of response to PD-1 blockade therapy, and that in experimental mouse models the T cell exclusion and anti-PD-1 resistance could be reversed by PAK4 inhibition (Abril-Rodríguez et al., 2020). In the CheckMate 038 biopsy dataset, *PAK4* expression did not differ significantly between baseline and on-treatment for patients with PD or SD, but expression was significantly (p < 2.7 × 10^{-4}) downregulated in on-treatment biopsies of patients with CRPR (after applying an optimal pooled t test, Figure 6J). This change was not explained by interferon-γ signaling, since in our melanoma cell line cohort, *PAK4* did not change significantly in response to interferon-γ. Interestingly, all of these biomarkers of immune exclusion were highly correlated, except for the T cell exclusion-up signature, which, as expected, was anti-correlated (Pearson correlation, Figure 6K). Together, these data indicate that ICB therapy results in decreased expression of immune exclusion gene programs in biopsies of patients who experience clinical response to therapy. While interferon-γ from T cells directly decreases *WNT* signaling and *MYC*, decreases in the Jerby-Arnon immune exclusion down signature, *CDK4*, or *PAK4* expression are likely downstream effects in clinically responding tumors.
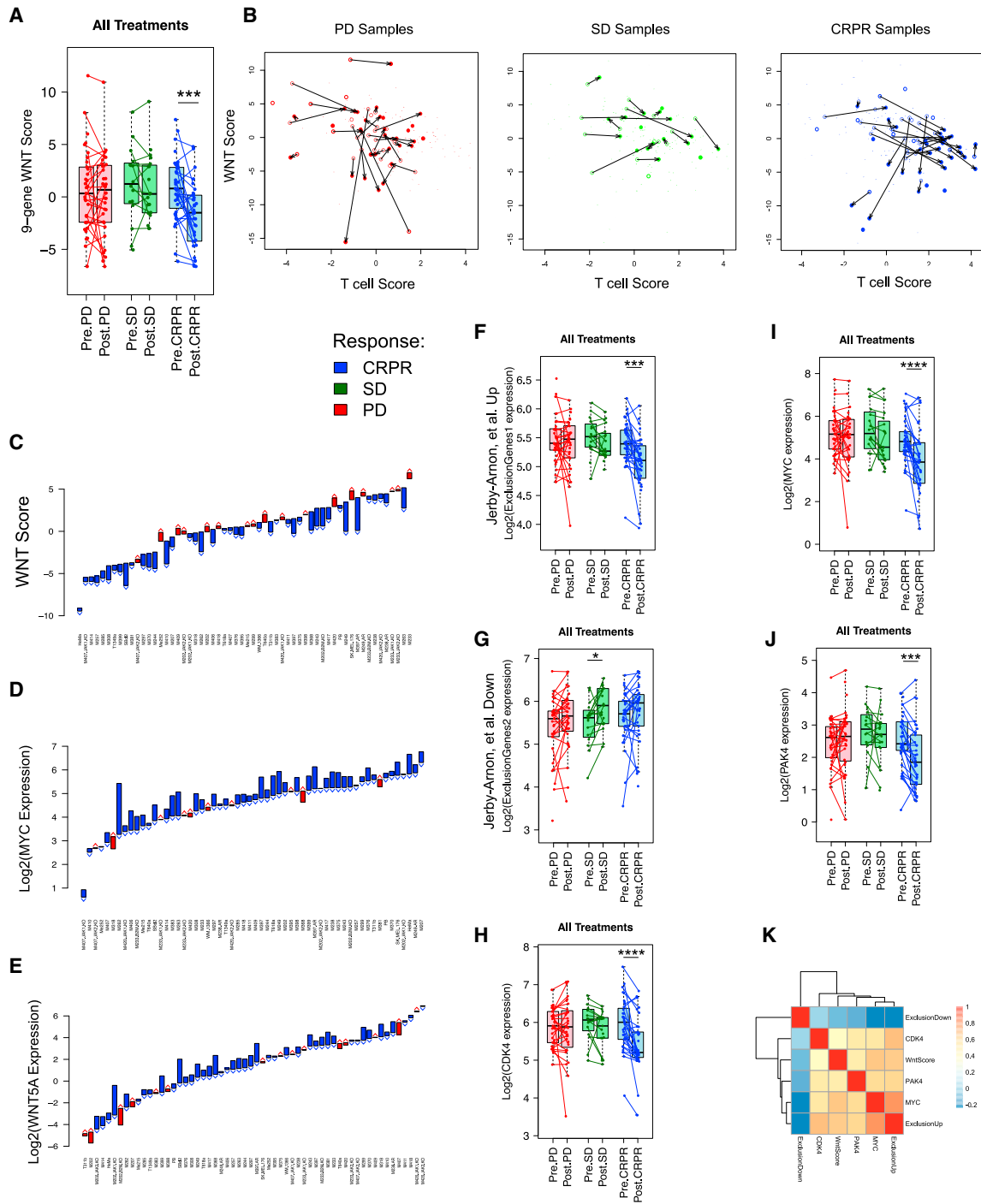
Figure 6. Immune Exclusion Signatures and WNT Signaling in Biopsies of Patients Receiving ICB Therapy

(A) Boxplot of the nine gene WNT score (the geometric average of *APC*, *APC2*, *CTNNB1*, *MYC*, *SOX11*, *SOX2*, *TCF12*, *TCF7*, and *VEGFA*), by RNA-seq according to response to therapy in patient biopsies using an optimal pooled t test since data are paired and unpaired (*p < 0.05, **p < 0.01, ***p < 0.001).

(B) Plot of WNT score versus T cell score with arrows connecting pre-treatment and on-treatment and one figure for each response PD (red), SD (green), and CRPR (blue).

(C–E) Pre- and post-treatment gene expression levels of the WNT score (C), *MYC* (D), and *WNT5A* (E), the WNT ligand initiating the downstream WNT signaling programming (red, up; blue, down).

(legend continued on next page)

DISCUSSION

Results from the current study provide a possible scenario by which response to ICB therapy, either PD-1 blockade alone or in combination with CTLA-4 blockade, can be explained by the development of a strong T cell response that can overcome immune cell-intrinsic, tumor-intrinsic, and tumor microenvironment limitations to a clinically effective antitumor immune response (Kalbasi and Ribas, 2020). Key contributing factors are: (1) the pre-existing level of T cell infiltration of the tumor (Herbst et al., 2014; Taube et al., 2014; Tumeh et al., 2014), which reflects both the immunogenicity of the cancer cells and the ability of the host immune system to have made a serious attempt to attack them specifically; (2) the baseline expression of immune suppressive gene programs by cancer cells that are detrimental to the initiation of an antitumor immune response, such as WNT signaling (Grasso et al., 2018; Spranger et al., 2015; Spranger and Gajewski, 2018); and (3) the strength of the antitumor immune response that results from the release of the immune checkpoint PD-1, alone or together with the checkpoint CTLA-4, driving the expression of interferon-γ response genes in the tumor microenvironment (Ayers et al., 2017; Cristescu et al., 2018). The release of interferon-γ from T cells recognizing cognate antigen on cancer cells serves to amplify the nascent antitumor immune response, which our and previous data (Neubert et al., 2017) suggest is mediated by the conserved ability of the great majority of melanoma cells to signal through the interferon-γ receptor. Amplification of the immune response is a result of an increase in antigen presentation machinery, positive feedback resulting in increased interferon-γ pathway signaling, production of chemokines that attract other immune cells favorably altering the tumor microenvironment and inhibition of immune exclusion cancer signatures.

The strength of the antitumor immune response depends on the interplay of these key contributing factors, which could be individually modulated with additional interventions as there does not seem to be a dominant process that would always inhibit mounting the antitumor response in the majority of cases without clinical response to ICB therapy. In preclinical modeling (Curran et al., 2010; Wei et al., 2017, 2019) and in clinical series (Larkin et al., 2019), the combination of anti-PD-1 and anti-CTLA-4 is arguably a stronger immune stimulation than either therapy alone, thereby shifting the balance in favor of an antitumor immune response in a greater number of cases. Another way to shift this balance would be to induce a physiological process of intratumoral interferon production by triggering pattern recognition receptors, such as the use of intratumoral administration of oncolytic viruses or Toll-like receptor agonists, two approaches already successfully reported to improve response rates of PD-1 blockade therapy (Ribas et al., 2018a, 2018b; Vanpouille-Box et al., 2019). Additional combinatorial approaches to enhance responses to ICB, not yet demonstrated to be clinically active in patients, include the triggering of the STING pathway (Li and Chen, 2018), inhibition of immune sup-

pressive factors, such as WNT signaling or the adenosine pathway (Abril-Rodríguez et al., 2020; Grasso et al., 2018; Smyth et al., 2016; Spranger and Gajewski, 2018), or the release of other immune checkpoints, such as LAG-3, TIM-3, or TIGIT, and others in T cells (Smyth et al., 2016). These observations provide hope that the benefit of cancer immunotherapy can be expanded to more patients and indications by using a combination therapy that reaches the level where antitumor T cells are potent enough to overcome the different nodes that restrict immune responses to cancer (Smyth et al., 2016).

It was possible that cancer cells may have different inherent abilities to respond to interferon-γ, and this may lead to some patients responding or not to ICB because some cancers may not induce the full set of interferon-γ response genes that are needed to mount a productive antitumor immune response. However, our data using a panel of melanoma cell lines suggest that this is very unlikely, at least in patients with metastatic melanoma. The data on interferon-γ response in these cell lines was dichotomous, clearly separating the cell lines with or without the ability to signal from the interferon-γ receptor. The cell lines unable to signal had natural or modeled homozygous loss-of-function mutations in *JAK1* or *JAK2*. These mutations can develop sporadically in patients with melanoma and other cancers before receiving ICB immunotherapy, but they are infrequent, likely less than 1% of the cases (Liu et al., 2019; Shin et al., 2017). Upon selective immune pressure they may become more frequent and lead to acquired resistance, but these seem to also be rather infrequent cases (Sucker et al., 2017; Zaretsky et al., 2016). Given the low baseline frequency of loss-of-function mutations in the interferon-γ signaling pathway, signaling through the interferon-γ receptor inducing the full set of interferon-γ response genes may be a positively selected feature of melanoma cells, which is rather counter-intuitive. At baseline, it may be favorable to the cancer cells to maintain this signaling and express immune suppressive molecules, such as PD-L1, indoleamine 2,3-dioxygenase, colony-stimulating factor 1, vascular endothelial growth factor, or interleukin-6, for example, to stop the antitumor immune response, but this is at the expense of making the cancer cells more vulnerable to a future immune response.

A common feature of biopsies from patients who respond to ICB is the expression of immune activation genes with mostly overlapping signatures (Ayers et al., 2017; Cristescu et al., 2018; Fehrenbacher et al., 2016; Jerby-Arnon et al., 2018; Liu et al., 2019; Rodig et al., 2018; Roh et al., 2017; Rooney et al., 2015; Sade-Feldman et al., 2018). Our studies suggest that the common denominator of these immune activation transcriptomes is the expression of interferon-γ response genes initiated by the activation of tumor antigen-specific T cells, which increases upon ICB. Key among these gene sets is the expression of antigen presenting machinery, most notably MHC class I and II, among biopsies of patients who go on to respond to ICB therapy (Liu et al., 2019; Rodig et al., 2018). This was the most relevant feature separating patients who responded or not to

---

(F–J) Boxplots of immune exclusion genes/signatures by RNA-seq according to response to therapy: Jerby-Arnon et al. associated immune exclusion gene set 1 up in immune excluded tissues (F) and set 2 down in immune excluded samples (G), CDK4 (H), MYC (I), and PAK4 (J) using an optimal pooled t test since data are paired and unpaired (*p < 0.05, **p < 0.01, ***p < 0.001).
(K) Heatmap showing the level of correlation between the immune exclusion genes and signatures.
See also Figures S19–S21.

therapy in our series, in particular the increase in MHC genes in on-therapy biopsies. However, a significant component of the increase in expression of *MHC* genes had to be from the infiltration with hematopoietic lineage cells into responding tumors as assessed by LCA correction. Therefore, future analyses would need to use techniques allowing determination of cancer cell-intrinsic antigen processing and presentation pathway.

The baseline expression of several T cell immune exclusion signatures has been associated with lack of response to ICB in different series, most of which also have overlapping gene sets (Auslander et al., 2018; Jerby-Arnon et al., 2018; Jiang et al., 2018; Liu et al., 2019). In our series, baseline and on-therapy biopsies of patients without a response to ICB therapy had a higher expression of the Jerby-Arnon et al. (2018) signatures of T cell exclusion, with the relevant feature that responding biopsies displayed decreases in expression of *WNT* and *MYC* genes on-therapy, while non-responding biopsies continued to express the immune exclusion genes. Overall, our data together with transcriptome analyses of other biopsy series (Auslander et al., 2018; Ayers et al., 2017; Cabrita et al., 2020; Chen et al., 2016; Cristescu et al., 2018; Fehrenbacher et al., 2016; Gide et al., 2019; Helmink et al., 2020; Hugo et al., 2016; Jerby-Arnon et al., 2018; Jiang et al., 2018; Liu et al., 2019; Petitprez et al., 2020; Riaz et al., 2017; Rodig et al., 2018; Roh et al., 2017; Sade-Feldman et al., 2018), implies the presence of feedback loops between the tumor and CD8 T cells mediated by interferon-γ that modulates immune exclusion secondary to WNT signaling (Luke et al., 2019).

In conclusion, T cell infiltration and expression of interferon-γ-regulated genes increase in biopsies of patients receiving ICB therapy regardless of clinical response, whereas the degree of HLA upregulation on-therapy and the decrease in expression of genes associated with immune exclusion are features of clinically responding biopsies. The difference between responsive and non-responsive melanomas does not seem to be due to an inherent ability of some cancer cells to respond differently to interferon-γ, as the quality of the interferon-γ response program was similar in the great majority of melanoma cell lines tested. As we did not have single cells for RNA-seq analyses, we were not able to directly determine if the same was true in the tumor biopsies. In most cases, ICB was able to change the transcriptome of melanoma biopsies, but it did so to different degrees that correlate with favorable changes in the immune cell infiltrate. The ability to provide a more powerful anti-melanoma immune response with combination ICB explains a higher rate of responses. This information also provides hope that additional combinatorial strategies may dial up the antitumor immune response to become clinically meaningful in more patients, in particular when combining ICB therapy with treatments that increase interferon signaling inside tumors to jump-start an antitumor immune response when it is not already pre-existing, such as the intratumoral administration of oncolytic viruses or nucleotide sequences that trigger pattern recognition receptors to produce interferons (Ribas et al., 2018a, 2018b; Torrejon et al., 2020; Vanpouille-Box et al., 2019).

STAR★METHODS

Detailed methods are provided in the online version of this paper and include the following:

- ● KEY RESOURCES TABLE
- ● RESOURCE AVAILABILITY
  - ○ Lead Contact
  - ○ Materials Availability
  - ○ Data and Code Availability
- ● EXPERIMENTAL MODEL AND SUBJECT DETAILS
  - ○ Clinical Trial and Biopsy Collections
  - ○ Human Melanoma Cell Lines
- ● METHODS DETAILS
  - ○ RNA Sequencing
  - ○ RNA Immune Deconvolution Using MCP-Counter
  - ○ Interferon-Gamma *In Vitro* Exposure and Transcriptome Analysis
- ● QUANTIFICATION AND STATISTICAL ANALYSIS
  - ○ Statistics and Survival Analysis

AUTHOR CONTRIBUTIONS

C.S.G. and A.R. designed the experiments and wrote the paper. C.S.G., P.R.-M., M.W.-R., D.M.P., V.A., S.L.T., V.E.V., D.E.S., A.K., and A.R. provided overall scientific oversight on the analyses. C.S.G., J.T., M.Q., G.A.-R., and E.M. performed bioinformatics analyses. M.O. and P.T. performed experimental studies. A.C., D.Y.T., D.S.S., Y.J.K., C.P.-S., K.C., A.V.-C., C.M., D.E.S., A.K., and A.R. provided specific expertise for bioinformatics data

interpretation. J.J.L., J.D.W., D.B.J., B.C., F.S.H., S.B., W.S., W.J.U., C.L.S., A.D., J.B.A.G.H., S.M.A., and A.R. collected patient samples.

REFERENCES

Abril-Rodríguez, G., Torrejon, D.Y., Liu, W., Zaretsky, J.M., Nowicki, T.S., Tsoi, J., Puig-Saus, C., Baselga Carretero, I., Medina, E., Quist, M.J., et al. (2020). PAK4 inhibition improves PD-1 blockade immunotherapy. Nat. Cancer *1*, 46–58.

Anders, S., Pyl, P.T., and Huber, W. (2015). HTSeq—a Python framework to work with high-throughput sequencing data. Bioinformatics 31, 166–169.

Atefi, M., Avramis, E., Lassen, A., Wong, D.J., Robert, L., Foulad, D., Cerniglia, M., Titz, B., Chodon, T., Graeber, T.G., et al. (2014). Effects of MAPK and PI3K pathways on PD-L1 expression in melanoma. Clin. Cancer Res. 20, 3446–3457.

Auslander, N., Zhang, G., Lee, J.S., Frederick, D.T., Miao, B., Moll, T., Tian, T., Wei, Z., Madan, S., Sullivan, R.J., et al. (2018). Robust prediction of response to immune checkpoint blockade therapy in metastatic melanoma. Nat. Med. 24, 1545–1549.

Ayers, M., Lunceford, J., Nebozhyn, M., Murphy, E., Loboda, A., Kaufman, D.R., Albright, A., Cheng, J.D., Kang, S.P., Shankaran, V., et al. (2017). IFN-gamma-related mRNA profile predicts clinical response to PD-1 blockade. J. Clin. Invest. 127, 2930–2940.

Bach, E.A., Aguet, M., and Schreiber, R.D. (1997). The IFN gamma receptor: a paradigm for cytokine receptor signaling. Annu. Rev. Immunol. 15, 563–591.

Becht, E., Giraldo, N.A., Lacroix, L., Buttard, B., Elarouci, N., Petitprez, F., Selves, J., Laurent-Puig, P., Sautes-Fridman, C., Fridman, W.H., et al. (2016). Estimating the population abundance of tissue-infiltrating immune and stromal cell populations using gene expression. Genome Biol. 17, 218.

Cabrita, R., Lauss, M., Sanna, A., Donia, M., Skaarup Larsen, M., Mitra, S., Johansson, I., Phung, B., Harbst, K., Vallon-Christersson, J., et al. (2020). Tertiary lymphoid structures improve immunotherapy and survival in melanoma. Nature 577, 561–565.

Chen, P.L., Roh, W., Reuben, A., Cooper, Z.A., Spencer, C.N., Prieto, P.A., Miller, J.P., Bassett, R.L., Gopalakrishnan, V., Wani, K., et al. (2016). Analysis of immune signatures in longitudinal tumor samples yields insight into biomarkers of response and mechanisms of resistance to immune checkpoint blockade. Cancer Discov. 6, 827–837.

Cristescu, R., Mogg, R., Ayers, M., Albright, A., Murphy, E., Yearley, J., Sher, X., Liu, X.Q., Lu, H., Nebozhyn, M., et al. (2018). Pan-tumor genomic biomarkers for PD-1 checkpoint blockade-based immunotherapy. Science 362, eaar3593.

Curran, M.A., Montalvo, W., Yagita, H., and Allison, J.P. (2010). PD-1 and CTLA-4 combination blockade expands infiltrating T cells and reduces regulatory T and myeloid cells within B16 melanoma tumors. Proc. Natl. Acad. Sci. U S A 107, 4275–4280.

Fehrenbacher, L., Spira, A., Ballinger, M., Kowanetz, M., Vansteenkiste, J., Mazieres, J., Park, K., Smith, D., Artal-Cortes, A., Lewanski, C., et al. (2016). Atezolizumab versus docetaxel for patients with previously treated non-small-cell lung cancer (POPLAR): a multicentre, open-label, phase 2 randomised controlled trial. Lancet 387, 1837–1846.

Garcia-Diaz, A., Shin, D.S., Moreno, B.H., Saco, J., Escuin-Ordinas, H., Rodriguez, G.A., Zaretsky, J.M., Sun, L., Hugo, W., Wang, X., et al. (2017). Interferon receptor signaling pathways regulating PD-L1 and PD-L2 expression. Cell Rep. 19, 1189–1201.

Gettinger, S., Choi, J., Hastings, K., Truini, A., Datar, I., Sowell, R., Wurtz, A., Dong, W., Cai, G., Melnick, M.A., et al. (2017). Impaired HLA class I antigen processing and presentation as a mechanism of acquired resistance to immune checkpoint inhibitors in lung cancer. Cancer Discov. 7, 1420–1435.

Gide, T.N., Quek, C., Menzies, A.M., Tasker, A.T., Shang, P., Holst, J., Madore, J., Lim, S.Y., Velickovic, R., Wongchenko, M., et al. (2019). Distinct immune cell populations define response to anti-PD-1 monotherapy and anti-PD-1/anti-CTLA-4 combined therapy. Cancer Cell 35, 238–255.e6.

Grasso, C.S., Giannakis, M., Wells, D.K., Hamada, T., Mu, X.J., Quist, M., Nowak, J.A., Nishihara, R., Qian, Z.R., Inamura, K., et al. (2018). Genetic mechanisms of immune evasion in colorectal cancer. Cancer Discov. 8, 730–749.

Guo, B., and Yuan, Y. (2017). A comparative review of methods for comparing means using partially paired data. Stat. Methods Med. Res. 26, 1323–1340.

Helmink, B.A., Reddy, S.M., Gao, J., Zhang, S., Basar, R., Thakur, R., Yizhak, K., Sade-Feldman, M., Blando, J., Han, G., et al. (2020). B cells and tertiary lymphoid structures promote immunotherapy response. Nature 577, 549–555.

Herbst, R.S., Soria, J.C., Kowanetz, M., Fine, G.D., Hamid, O., Gordon, M.S., Sosman, J.A., McDermott, D.F., Powderly, J.D., Gettinger, S.N., et al. (2014).

Predictive correlates of response to the anti-PD-L1 antibody MPDL3280A in cancer patients. Nature 515, 563–567.

Hugo, W., Zaretsky, J.M., Sun, L., Song, C., Moreno, B.H., Hu-Lieskovan, S., Berent-Maoz, B., Pang, J., Chmielowski, B., Cherry, G., et al. (2016). Genomic and transcriptomic features of response to anti-PD-1 therapy in metastatic melanoma. Cell 165, 35–44.

Jerby-Arnon, L., Shah, P., Cuoco, M.S., Rodman, C., Su, M.J., Melms, J.C., Leeson, R., Kanodia, A., Mei, S., Lin, J.R., et al. (2018). A cancer cell program promotes T cell exclusion and resistance to checkpoint blockade. Cell 175, 984–997.e24.

Jiang, P., Gu, S., Pan, D., Fu, J., Sahu, A., Hu, X., Li, Z., Traugh, N., Bu, X., Li, B., et al. (2018). Signatures of T cell dysfunction and exclusion predict cancer immunotherapy response. Nat. Med. 24, 1550–1558.

Kalbasi, A., and Ribas, A. (2020). Tumour-intrinsic resistance to immune checkpoint blockade. Nat. Rev. Immunol. 20, 25–39.

Kim, D., Paggi, J.M., Park, C., Bennett, C., and Salzberg, S.L. (2019). Graph-based genome alignment and genotyping with HISAT2 and HISAT-genotype. Nat. Biotechnol. 37, 907–915.

Larkin, J., Chiarion-Sileni, V., Gonzalez, R., Grob, J.J., Rutkowski, P., Lao, C.D., Cowey, C.L., Schadendorf, D., Wagstaff, J., Dummer, R., et al. (2019). Five-year survival with combined nivolumab and ipilimumab in advanced melanoma. N. Engl. J. Med. 381, 1535–1546.

Li, T., and Chen, Z.J. (2018). The cGAS-cGAMP-STING pathway connects DNA damage to inflammation, senescence, and cancer. J. Exp. Med. 215, 1287–1299.

Liu, D., Schilling, B., Liu, D., Sucker, A., Livingstone, E., Jerby-Amon, L., Zimmer, L., Gutzmer, R., Satzger, I., Loquai, C., et al. (2019). Integrative molecular and clinical modeling of clinical outcomes to PD1 blockade in patients with metastatic melanoma. Nat. Med. 25, 1916–1927.

Luke, J.J., Bao, R., Sweis, R.F., Spranger, S., and Gajewski, T.F. (2019). WNT/beta-catenin pathway activation correlates with immune exclusion across human cancers. Clin. Cancer Res. 25, 3074–3083.

Nazarian, R., Shi, H., Wang, Q., Kong, X., Koya, R.C., Lee, H., Chen, Z., Lee, M.K., Attar, N., Sazegar, H., et al. (2010). Melanomas acquire resistance to B-RAF(V600E) inhibition by RTK or N-RAS upregulation. Nature 468, 973–977.

Neubert, N.J., Tille, L., Barras, D., Soneson, C., Baumgaertner, P., Rimoldi, D., Gfeller, D., Delorenzi, M., Fuertes Marraco, S.A., and Speiser, D.E. (2017). Broad and conserved immune regulation by genetically heterogeneous melanoma cells. Cancer Res. 77, 1623–1636.

Nsengimana, J., Laye, J., Filia, A., O'Shea, S., Muralidhar, S., Pozniak, J., Droop, A., Chan, M., Walker, C., Parkinson, L., et al. (2018). beta-Catenin-mediated immune evasion pathway frequently operates in primary cutaneous melanomas. J. Clin. Invest. 128, 2048–2063.

Petitprez, F., de Reynies, A., Keung, E.Z., Chen, T.W., Sun, C.M., Calderaro, J., Jeng, Y.M., Hsiao, L.P., Lacroix, L., Bougouin, A., et al. (2020). B cells are associated with survival and immunotherapy response in sarcoma. Nature 577, 556–560.

Riaz, N., Havel, J.J., Makarov, V., Desrichard, A., Urba, W.J., Sims, J.S., Hodi, F.S., Martin-Algarra, S., Mandal, R., Sharfman, W.H., et al. (2017). Tumor and microenvironment evolution during immunotherapy with nivolumab. Cell 171, 934–949.e916.

Ribas, A., Dummer, R., Puzanov, I., VanderWalde, A., Andtbacka, R.H.I., Michielin, O., Olszanski, A.J., Malvehy, J., Cebon, J., Fernandez, E., et al. (2018a). Oncolytic virotherapy promotes intratumoral T cell infiltration and improves anti-PD-1 immunotherapy. Cell 174, 1031–1032.

Ribas, A., Medina, T., Kummar, S., Amin, A., Kalbasi, A., Drabick, J.J., Barve, M., Daniels, G.A., Wong, D.J., Schmidt, E.V., et al. (2018b). SD-101 in combination with pembrolizumab in advanced melanoma: results of a phase Ib, multicenter study. Cancer Discov. 8, 1250–1257.

Ribas, A., and Wolchok, J.D. (2018). Cancer immunotherapy using checkpoint blockade. Science 359, 1350–1355.

Rodig, S.J., Gusenleitner, D., Jackson, D.G., Gjini, E., Giobbie-Hurder, A., Jin, C., Chang, H., Lovitch, S.B., Horak, C., Weber, J.S., et al. (2018). MHC proteins

confer differential sensitivity to CTLA-4 and PD-1 blockade in untreated metastatic melanoma. Sci. Transl. Med. *10*, eaar3342.

Roh, W., Chen, P.L., Reuben, A., Spencer, C.N., Prieto, P.A., Miller, J.P., Gopalakrishnan, V., Wang, F., Cooper, Z.A., Reddy, S.M., et al. (2017). Integrated molecular analysis of tumor biopsies on sequential CTLA-4 and PD-1 blockade reveals markers of response and resistance. Sci. Transl. Med. *9*, eaah3560.

Rooney, M.S., Shukla, S.A., Wu, C.J., Getz, G., and Hacohen, N. (2015). Molecular and genetic properties of tumors associated with local immune cytolytic activity. Cell *160*, 48–61.

Sade-Feldman, M., Jiao, Y.J., Chen, J.H., Rooney, M.S., Barzily-Rokni, M., Eliane, J.P., Bjorgaard, S.L., Hammond, M.R., Vitzthum, H., Blackmon, S.M., et al. (2017). Resistance to checkpoint blockade therapy through inactivation of antigen presentation. Nat. Commun. *8*, 1136.

Sade-Feldman, M., Yizhak, K., Bjorgaard, S.L., Ray, J.P., de Boer, C.G., Jenkins, R.W., Lieb, D.J., Chen, J.H., Frederick, D.T., Barzily-Rokni, M., et al. (2018). Defining T cell states associated with response to checkpoint immunotherapy in melanoma. Cell *175*, 998–1013 e1020.

Sharma, A., Subudhi, S.K., Blando, J., Vence, L., Wargo, J., Allison, J.P., Ribas, A., and Sharma, P. (2019). Anti-CTLA-4 immunotherapy does not deplete FOXP3(+) regulatory T cells (Tregs) in human cancers-response. Clin. Cancer Res. *25*, 3469–3470.

Sharma, P., and Allison, J.P. (2015a). The future of immune checkpoint therapy. Science *348*, 56–61.

Sharma, P., and Allison, J.P. (2015b). Immune checkpoint targeting in cancer therapy: toward combination strategies with curative potential. Cell *161*, 205–214.

Shin, D.S., Zaretsky, J.M., Escuin-Ordinas, H., Garcia-Diaz, A., Hu-Lieskovan, S., Kalbasi, A., Grasso, C.S., Hugo, W., Sandoval, S., Torrejon, D.Y., et al. (2017). Primary resistance to PD-1 blockade mediated by JAK1/2 mutations. Cancer Discov. *7*, 188–201.

Smyth, M.J., Ngiow, S.F., Ribas, A., and Teng, M.W. (2016). Combination cancer immunotherapies tailored to the tumour microenvironment. Nat. Rev. Clin. Oncol. *13*, 143–158.

Sondergaard, J.N., Nazarian, R., Wang, Q., Guo, D., Hsueh, T., Mok, S., Sazegar, H., Macconaill, L.E., Barretina, J.G., Kehoe, S.M., et al. (2010). Differential sensitivity of melanoma cell lines with BRAFV600E mutation to the specific raf inhibitor PLX4032. J. Transl Med. *8*, 39.

Spranger, S., Bao, R., and Gajewski, T.F. (2015). Melanoma-intrinsic beta-catenin signalling prevents anti-tumour immunity. Nature *523*, 231–235.

Spranger, S., and Gajewski, T.F. (2018). Impact of oncogenic pathways on evasion of antitumour immune responses. Nat. Rev. Cancer *18*, 139–147.

Sucker, A., Zhao, F., Pieper, N., Heeke, C., Maltaner, R., Stadtler, N., Real, B., Bielefeld, N., Howe, S., Weide, B., et al. (2017). Acquired IFNgamma resistance impairs anti-tumor immunity and gives rise to T-cell-resistant melanoma lesions. Nat. Commun. *8*, 15440.

Taube, J.M., Klein, A.P., Brahmer, J.R., Xu, H., Pan, X., Kim, J.H., Chen, L., Pardoll, D.M., Topalian, S.L., and Anders, R.A. (2014). Association of PD-1, PD-1 ligands, and other features of the tumor immune microenvironment with response to anti-PD-1 therapy. Clin. Cancer Res. *20*, 5064–5074.

Torrejon, D.Y., Abril-Rodriguez, G., Champhekar, A.S., Tsoi, J., Campbell, K.M., Kalbasi, A., Parisi, G., Zarestsky, J.M., Garcia-Diaz, A., Puig-Saus, C., et al. (2020). Overcoming genetically-based resistance mechanisms to PD-1 blockade. Cancer Discov. *10*, 1140–1157.

Tsoi, J., Robert, L., Paraiso, K., Galvan, C., Sheu, K., Lay, J., Wong, D.J.L., Atefi, M., Shirazi, R., Wang, X., et al. (2018). Multi-stage differentiation defines melanoma subtypes with differential vulnerability to drug-induced iron-dependent oxidative stress. Cancer Cell *33*, 890–904.e5.

Tumeh, P.C., Harview, C.L., Yearley, J.H., Shintaku, I.P., Taylor, E.J., Robert, L., Chmielowski, B., Spasic, M., Henry, G., Ciobanu, V., et al. (2014). PD-1 blockade induces responses by inhibiting adaptive immune resistance. Nature *515*, 568–571.

Vanpouille-Box, C., Hoffmann, J.A., and Galluzzi, L. (2019). Pharmacological modulation of nucleic acid sensors—therapeutic potential and persisting obstacles. Nat. Rev. Drug Discov. *18*, 845–867.

Wei, S.C., Anang, N.A.S., Sharma, R., Andrews, M.C., Reuben, A., Levine, J.H., Cogdill, A.P., Mancuso, J.J., Wargo, J.A., Pe'er, D., et al. (2019). Combination anti-CTLA-4 plus anti-PD-1 checkpoint blockade utilizes cellular mechanisms partially distinct from monotherapies. Proc. Natl. Acad. Sci. U S A *116*, 22699–22709.

Wei, S.C., Levine, J.H., Cogdill, A.P., Zhao, Y., Anang, N.A.S., Andrews, M.C., Sharma, P., Wang, J., Wargo, J.A., Pe'er, D., et al. (2017). Distinct cellular mechanisms underlie anti-CTLA-4 and anti-PD-1 checkpoint blockade. Cell *170*, 1120–1133.e17.

Zaretsky, J.M., Garcia-Diaz, A., Shin, D.S., Escuin-Ordinas, H., Hugo, W., Hu-Lieskovan, S., Torrejon, D.Y., Abril-Rodriguez, G., Sandoval, S., Barthly, L., et al. (2016). Mutations associated with acquired resistance to PD-1 blockade in melanoma. N. Engl. J. Med. *375*, 819–829.

STAR★METHODS

KEY RESOURCES TABLE

REAGENT or RESOURCE	SOURCE	IDENTIFIER
Biological Samples		
Patient tumor biopsies collected from advanced melanoma patients in clinical study CheckMate 038	This article	https://clinicaltrials.gov/ct2/show/NCT01621490
Chemicals, Peptides, and Recombinant Proteins		
Recombinant Human IFN-gamma	BD Biosciences	Cat No. 554617
Critical Commercial Assays		
RNA extraction with miRNeasy Mini Kit	Qiagen	Cat No. 217004
Illumina Truseq Stranded mRNA kit	Illumina	https://www.illumina.com/products/by-type/sequencing-kits/library-prep-kits/truseq-stranded-mrna.html Cat No. 20020595
Deposited Data		
Checkmate-038 biopsies RNAseq raw and analyzed data	This paper	European Genome-phenome Archive CM38_DNA - EGAS00001004548 CM38_RNA - EGAS00001004545
M series human melanoma cell line RNAseq raw and analyzed data, with and without interferon-gamma exposure	This paper	Gene Expression Omnibus (GEO) GSE154996 https://www.ncbi.nlm.nih.gov/geo/query/acc.cgi?acc=GSE154996
Experimental Models: Cell Lines		
Human: M-series patient derived cell lines	This paper; Drs. James Economou, Antoni Ribas, and Roger Lo Labs	Sondergaard et al., 2010
Human: Primary Epidermal Melanocytes; Normal, Adult (HEMa)	ATCC	PCS-200-013
Software and Algorithms		
HISAT2 (v.2.0.5)	(Kim et al., 2019)	https://ccb.jhu.edu/software/hisat2/index.shtml
HTSeq (0.6.1)	(Anders et al., 2015)	https://ccb.jhu.edu/software/hisat2/index.shtml
R (v3.2)	N/A	https://www.r-project.org/
MCPcounter R Package	N/A	https://github.com/ebecht/MCPcounter

RESOURCE AVAILABILITY

Lead Contact
Further information and requests for resources and reagents should be directed to and will be fulfilled by the Lead Contact, Antoni Ribas (aribas@mednet.ucla.edu).

Materials Availability
Melanoma cell lines are available from the Lead Contact with a completed Materials Transfer Agreement following institutional policies.

Data and Code Availability
RNA-seq data from patients who consented to deposition has been deposited in the European Genome-phenome Archive, with accession numbers CM38_DNA - EGAS00001004548 and CM38_RNA - EGAS00001004545. The RNA-seq data for human melanoma cell lines with and without interferon-gamma exposure for 6-hours is deposited in the Gene Expression Omnibus (GEO), with accession number GSE154996. Both are listed in the Key Resources Table.

EXPERIMENTAL MODEL AND SUBJECT DETAILS

Clinical Trial and Biopsy Collections

Study CheckMate 038 (NCT01621490) was a multi-arm, multi-institutional, prospective study to investigate the effects of nivolumab (3 mg/kg every 2 weeks) single agent, or the combination of nivolumab (1 mg/kg every 3 weeks) plus ipilimumab (3 mg/kg every 3 weeks) given for four doses and followed by nivolumab (3 mg/kg every 2 weeks) single agent. The protocol and its amendments were approved by the relevant institutional review boards, and the study was conducted in accordance with the Declaration of Helsinki and the International Conference on Harmonization Guidelines for Good Clinical Practice. All patients signed written informed consent prior to having any study procedures performed. Patients were treated until progression or for a maximum of 2 years, or were stopped due to toxicities. Radiographic assessment of response was performed approximately every 8 weeks until progression. Progression was confirmed with a repeat CT scan at least four weeks later. Tumor response for patients was defined by RECIST v1.1. Response to therapy indicates best overall response unless otherwise indicated. All patients underwent a baseline biopsy before commencing therapy (1 to 7 days before the first dose of therapy) and a repeat biopsy, on cycle 1, day 29 (between days 23–29).

Human Melanoma Cell Lines

Human melanoma cell lines were established from patient's biopsies under UCLA IRB approval # 11–003254 as previously described (Atefi et al., 2014; Nazarian et al., 2010; Sondergaard et al., 2010; Tsoi et al., 2018).

METHODS DETAILS

RNA Sequencing

Tumor tissue was divided for formalin-fixed paraffin-embedding (FFPE) for IHC analysis, and storage with RNAlater (Ambion) for subsequent RNA extraction using Qiagen kits. Of 170 patients, 101 had enough RNA for RNAseq. RNAseq library was prepared using Illumina Truseq Stranded mRNA kit. Sequencing was done on an Illumina Hiseq sequencer using paired end sequencing of 50 bp for each mate pair. RNAseq reads were mapped using HISAT2 version 2.0.4 (Kim et al., 2019) and aligned to the hg19 genome using default parameters. Reads were quantified by HTSeq version 0.6.1 (Anders et al., 2015) with the intersection-non-empty mode and counting ambiguous reads if fully overlapping. Raw counts were then normalised to fragments per kilobase of exon per million fragments mapped (FPKM) expression values. Heatmaps of log2 FPKM expression data and z-scores were generated using the pheatmap R package. Progression free and overall survival plots were generated using the survival and ggsurv R packages. For melanoma cell line RNAseq analysis with and without interferon-gamma exposure, RNAseq reads were mapped using HISAT2 version 2.0.4 (Kim et al., 2019) and aligned to the hg19 genome using default parameters. Reads were quantified by HTSeq version 0.6.1 (Anders et al., 2015) with the intersection-non-empty mode and counting ambiguous reads if fully overlapping. Raw counts were then normalized to fragments per FPKM expression values.

RNA Immune Deconvolution Using MCP-Counter

RNA sequencing (RNA-seq)–based cell deconvolution of tissue-infiltrating immune and stromal populations using MCP-counter (Becht et al., 2016),based on 111 genes, including *CD8A* and *ICOS*, two genes in the T cell average measurement, was applied to all the samples to assess tumor infiltration of T cells, cytotoxic lymphocytes, CD8 T cells, myeloid dendritic cells, monocytic lineages, B lineage cells, NK cells, endothelial cells and fibroblast cells. A key advantage of MCP-Counter is that it accounts for the tumor cell fraction. As a result, T cell average from MCP-Counter is correlated with tumor-infiltrating lymphocyte (TIL) score, a pathology-based measure of T cell infiltration, based on 429 pathology slides available for TCGA samples (Grasso et al., 2018). This measurement is highly correlated with *CD8A* expression by itself (R^2 = 0.73) and the "CYT" score (the average of *GZMA* and *PRF1* expression, a measure of immune cytolytic activity based on two genes not present in the T cell average) (Rooney et al., 2015). We use the measurement with more genes here for robustness and for consistency with recent analyses, in addition, the including of stromal populations increases the overall accuracy.

Interferon-Gamma *In Vitro* Exposure and Transcriptome Analysis

Melanoma cell lines were seeded on 10 cm tissue culture plates in RPMI media with 10% FBS and 1% PSA. After allowing 2-3 passages during exponential growth phase at 70% confluence cells were exposed to interferon-gamma at concentration 5 ng/ml (Recombinant Human IFN-gamma, 0.1-2.0x10⁸ units/mg, BD Biosciences, Cat No. 554617). Culture media without interferon-gamma was added simultaneously to the controls. Cells were collected, cell pellets were frozen immediately and stored at -80°C. RNA was extracted with miRNeasy Mini Kit (Qiagen, Cat No. 217004). RNA sequencing was performed on Illumina HiSeq 3000, with a 1x50 run and with data quality check done on Illumina SAV and demultiplexing performed with Illumina Bcl2fastq2 v 2.17 program.

QUANTIFICATION AND STATISTICAL ANALYSIS

Statistics and Survival Analysis

Statistical analyses were performed in R. Paired t-tests were used on the melanoma cell lines before and after interferon gamma treatment. The patient data is a combination of paired and unpaired observations (partially paired data), so we used the "optimal pooled t-test" described by Guo and Yuan in their comparative review of such methods (Guo and Yuan, 2017). An FDR was applied when we used either t-test to all the genes in a cohort in order to yield a list of significantly altered genes. An FDR was not applied when we looked at individual genes that we selected on the basis of biological interest, which is standard practice.